

Gate-Control of Spin Precession in Quantum Hall Edge States

T. Nakajima,^{1,*} Kuan-Ting Lin,² and S. Komiyama¹

¹Department of Basic Science, University of Tokyo, Komaba, Meguro-ku, Tokyo 153-8902, Japan

²Department of Physics, National Tsing Hua University, Hsinchu 30013, Taiwan

Electrical control and detection of spin precession are experimentally demonstrated by using spin-resolved edge states in the integer quantum Hall regime. Spin precession is triggered at a corner of a biased metal gate, where electron orbital motion makes a sharp turn leading to a nonadiabatic change in the effective magnetic field via spin-orbit interaction. The phase of precession is controlled by the group velocity of edge-state electrons tuned by gate bias voltage: A spin-FET device is thus realized by all-electrical means, without invoking ferromagnetic material. The effect is also interpreted in terms of a Mach-Zehnder-type spin interferometer.

PACS numbers: 73.43.Fj, 85.75.Hh, 72.25.Dc

Electrical control of electron spin is a key element for realizing spin-based quantum information processing in solid-state devices. Spin-orbit interaction (SOI) has been exploited for manipulating single spins in quantum dots through alternating electric fields[1, 2]. Datta and Das proposed a novel framework for spin manipulation called spin-FET, in which spin precession of moving electrons in a 1D system is controlled only by *constant* electric fields[3, 4]. This approach provides a realistic scheme for building an electronic analogue of photonic quantum information processing[5–10] in solid-state systems: Quantum logic gates may be implemented in a coherent circuit by encoding *flying qubits* in the spin degree of freedom of ballistic electrons.

Edge states in the quantum Hall regime is an ideal 1D electron system for this purpose because of its large equilibration length[11, 12] and long-range quantum mechanical coherence[13]. Moreover, spin-polarized current can be selectively injected and detected by controlling gate bias conditions[14–16] without resort to ferromagnetic leads assumed in the original proposal of the spin-FET[3]. Indeed, control of spin precession in edge states has been theoretically discussed[17–21], but no experimental realization has been reported so far.

In this Letter, we demonstrate *all-electrical* spin-FET-like control of spin precession in edge states. The key is a non-uniform arrangement of SOI-induced magnetic field B_{SO} prepared in a tailored geometry of edge states (see Fig. 1(b)). Spin-polarized edge states are quantized in the effective magnetic field $B_{eff} = B_{SO} + B$ with B being the external magnetic field. Incoming electrons in a spin eigenstate for $B_{eff} = B_i$ are guided to a corner of a biased metal gate, at which B_{eff} changes to B_p nonadiabatically because B_{SO} changes its direction along with the sharp turn of electron drift motion[22, 23]. The spin state hence starts to evolve or precess around the axis of B_p . The spin precession continues until the electrons arrive at the opposite corner of the gate, where the up- and down-spin branches are separated. The projection of their final state onto the up-spin eigenstate for $B_{eff} = B_f$ is read out by the Hall voltage. The phase of precession is determined

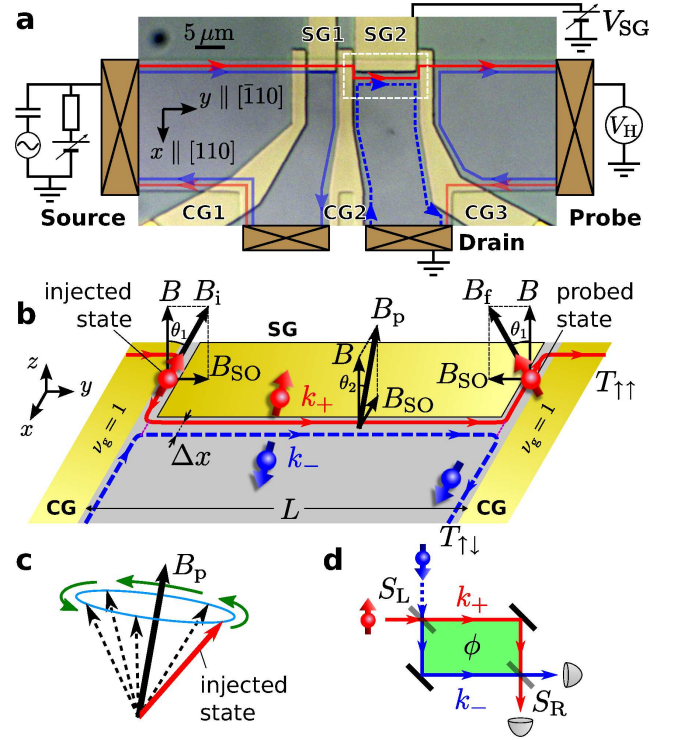


Figure 1. (Color online) (a) Optical microscope image of the device studied, together with a schematic of the experimental setup. Up- and down-spin edge states in the lowest Landau level are drawn in red and blue lines, respectively. (b) Schematic view of the region bounded by a white rectangle in (a). (c) Spin precession during the propagation along the side gate. (d) Schematic representation of an equivalent Mach-Zehnder-type spin interferometer.

by the Larmor frequency and the group velocity, which can be experimentally controlled by B and the gate bias voltage, respectively.

Devices were fabricated in GaAs/AlGaAs heterostructure crystals I and II[24]. Similar experimental results were obtained in the two, and only the results of crystal I will be described below for reasons of space. Figure 1(a) shows the optical microscope image of the device with

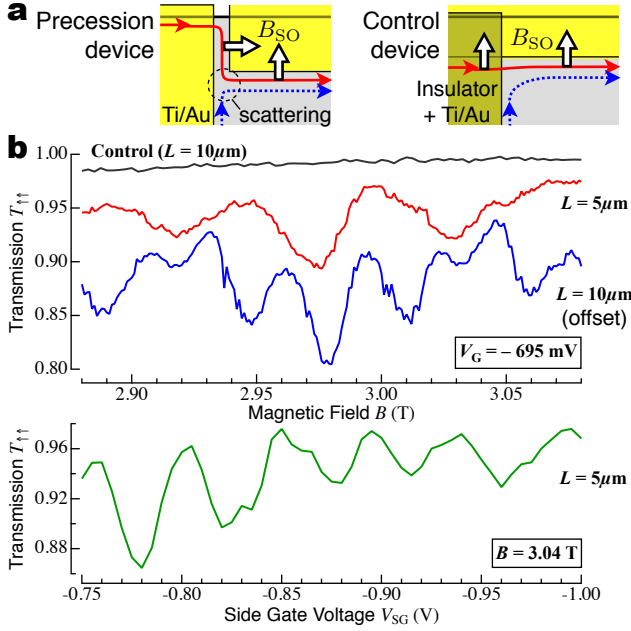


Figure 2. (Color online) (a) Schematics of the device in Fig. 1 (left) and the control device (right), focusing on the region where two edge states encounter with each other. (b) $T_{\uparrow\uparrow}$ against B (upper panel) and V_{SG} (lower panel).

three cross gates (CGs 1-3) and two side gates (SGs 1 and 2). The filling factor of Landau levels (LLs) in the bulk region is set to be $\nu = 3.7-2.5$ in magnetic fields of $B = 2.7-4.0$ T perpendicular to the 2D electron system at 100 mK. Only the spin-resolved edge states in the lowest LL are relevant to the experimental results because the edge states in higher LLs are completely decoupled and grounded. Two regions defined by CG1, CG2, SG1 (with length $L = 5 \mu\text{m}$) and by CG2, CG3, SG2 ($L = 10 \mu\text{m}$) are studied separately. Figure 1(a) depicts edge-state trajectories with $V_{CG1} = V_{SG1} = 0$ and $V_{CG2}, V_{CG3}, V_{SG2} < 0$ for studying the region of $L = 10 \mu\text{m}$. Electrons emitted from the source (drain) contact in the spin-up outer (spin-down inner) edge states are totally transmitted through (reflected at) CG2, biased so that $\nu_g = 1$ in the region below the gate. The transmitted electrons change the direction of motion at the left-hand corner of SG2 ($V_{SG} < -0.4$ V), start spin precession, and travel along the boundary of SG2 (see Fig. 1(b) and 2(a)). Reaching the right-hand corner of SG2, the electrons are partly transmitted (reflected) with probability $T_{\uparrow\uparrow}$ ($T_{\uparrow\downarrow} = 1 - T_{\uparrow\uparrow}$), which is experimentally probed by $T_{\uparrow\uparrow} = V_H/V_S$ with V_H and V_S being the Hall and the source voltages[14–16]. The voltage V_H is studied via a lock-in technique by superposing an ac component ($V_{ac} = 12.9 \mu\text{V}$ at 130 Hz) to a dc background ($V_{dc} = -103 \mu\text{V}$) in the source voltage ($V_S = V_{ac} + V_{dc}$)[24].

The spin precession manifests itself as distinct oscilla-

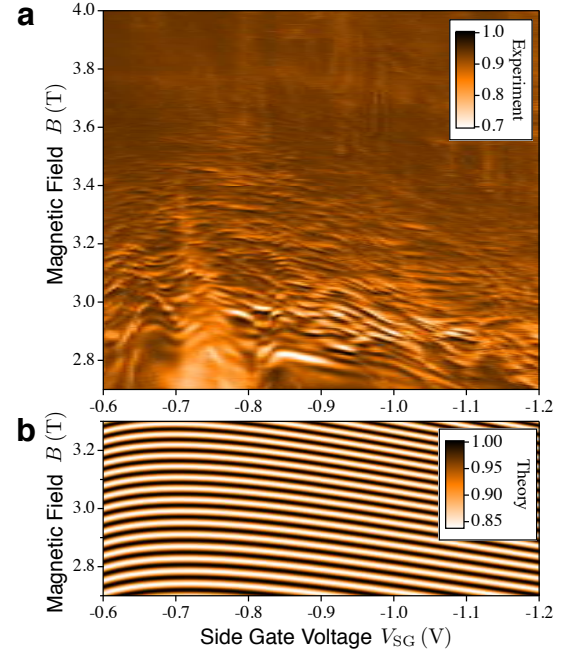


Figure 3. (Color online) Two-dimensional plot of $T_{\uparrow\uparrow}$ on the B - V_{SG} plane. (a) Experimental results obtained in the device of $L = 10 \mu\text{m}$. (b) Theoretical results derived from eq. (2) with $g = -2.9$, $C_0 = 0.92$, $C_1 = 0.08$ and $\phi_0 = 0$.

tions in $T_{\uparrow\uparrow}$ against B , as displayed in the upper panel of Fig. 2(b). The oscillation is visible both in the $10 \mu\text{m}$ - and the $5 \mu\text{m}$ -long regions[24], where the oscillation period for the latter is approximately twice as large as that for the former. The oscillation shows up also as a function of V_{SG} at a fixed B (lower panel of Fig. 2(b)).

To make explicit the essential role of the side-gate corners, a control experiment was made on another device shown in the right panel of Fig. 2(a), where the sharp turn of electron motion is prevented at the left end of the SG region. The device is prepared with CGs and SG overlapping with each other by introducing an insulation layer in between[24]. The oscillatory behavior is completely absent in the control experiment, as exemplified by the topmost line in Fig. 2(b). This provides compelling evidence that the oscillation of $T_{\uparrow\uparrow}$ is triggered by the nonadiabatic change of B_{SO} induced at the left corner of SG. In addition, the values of $T_{\uparrow\uparrow}$ in the control device are close to unity ($T_{\uparrow\uparrow} \approx 0.99$), being almost independent of B (and of V_{SG} though not shown here). The nearly perfect transmission indicates macroscopic equilibration lengths[11, 12], $\ell_{eq} \sim 300 \mu\text{m} \gg L$ in the present experiment, suggesting that the electrons are practically free from impurity-induced spin-flip scattering.

Figure 3(a) displays a two-dimensional plot of $T_{\uparrow\uparrow}(B, V_{SG})$ for $L = 10 \mu\text{m}$. The oscillatory pattern is visible in a wide range of B and V_{SG} such that $B = 2.7-3.5$ T and $V_{SG} = -0.6-1.2$ V. Although the pattern is disturbed to some extent by irregular structures, general

trend of oscillation is evident and the overall feature is distinctly different from the well-known irregular structure due to impurity-induced scattering[24].

For quantitative interpretation, we take into account two components of SOI in GaAs/AlGaAs heterostructures; namely, Rashba and Dresselhaus terms[25]. The two terms are of comparable strengths, and the Hamiltonian of each is given by $H_R = \alpha(p_y\sigma_x - p_x\sigma_y)/\hbar$ and $H_D = \beta(p_y\sigma_x + p_x\sigma_y)/\hbar$ in the coordinate system of $x \parallel [110]$, $y \parallel [\bar{1}10]$, and $z \parallel [001]$. Here p_i is the electron momentum and σ_i is the Pauli matrix ($i = x, y, \text{ or } z$). These terms yield the effective magnetic field $\mathbf{B}_{SO} = (2\alpha'p_y/(g\mu_B\hbar), 2\beta'p_x/(g\mu_B\hbar), 0)$, with g the effective g -factor ($g < 0$), μ_B the Bohr magneton, $\alpha' = \alpha + \beta$, and $\beta' = -\alpha + \beta$ ($|\alpha'| \gg |\beta'|$, $\beta' < 0$). This representation proves to be valid for edge states when \mathbf{p} is replaced with $m\mathbf{v}_g$, where m and \mathbf{v}_g are the effective mass and the group velocity of edge-state electrons[22, 23]. In the device studied (Fig. 1(b)), \mathbf{B}_{SO} changes from $(0, B_{SOi}, 0)$ to $(B_{SOp}, 0, 0)$ at the left-hand corner of SG where $B_{SOi} = 2\beta'm|\mathbf{v}_g|/(g\mu_B\hbar)$ and $B_{SOp} = 2\alpha'm|\mathbf{v}_g|/(g\mu_B\hbar)$. The spinor of the incoming electrons is given by $|i\rangle = R_x(-\theta_1)|\uparrow\rangle$ where $|\uparrow\rangle$ is the eigenstate of σ_z , $R_i(\theta)$ is the rotation operator about the i -axis, and $\theta_1 = \arctan(B_{SOi}/B)$. After turning the corner, the up- and the down-spin branches along the SG boundary are similarly given by $|+\rangle = R_y(-\theta_2)|\uparrow\rangle$ and $|-\rangle = R_y(-\theta_2)|\downarrow\rangle$ with $\theta_2 = \arctan(B_{SOp}/B)$. Hence, the initial state $|i\rangle$ becomes a superposition $a|+\rangle + b|-\rangle$ at the corner where the direction of \mathbf{v}_g changes nonadiabatically[26]. In other words, coherent inter-edge state scattering is caused by the local electric field at the gate corner via the SOI[22, 23]. In the control device, $\mathbf{B}_{SO} = (B_{SO}, 0, 0)$ is invariable with $B_{SO} = 2\alpha'm|\mathbf{v}_g|/(g\mu_B\hbar)$ along SG (Fig. 2(a)) so that the spin state is kept unchanged.

The up- and down-spin branches, $|+\rangle$ and $|-\rangle$, are associated with quasi-one-dimensional electron waves that propagate along the SG boundary (in the y -direction) with different wave numbers $k_{\pm} = -x_{\pm}/\ell_B^2$, where $\ell_B = \sqrt{\hbar/(eB)} \sim 15\text{ nm}$ is the magnetic length. The wave functions of the edge states are given by $\varphi_{k\pm}(x, y) = \frac{1}{\sqrt{L}}e^{ik_{\pm}y}\chi_0(x - x_{\pm})|\pm\rangle$ [27], where $\chi_0(x - x_{\pm}) \propto \exp(-(x - x_{\pm})^2/2\ell_B^2)$ describes the x -profile about the center coordinates $x = x_{\pm}$. During the propagation, the state evolves as $|\psi(y)\rangle = ae^{ik_+y}|+\rangle + be^{ik_-y}|-\rangle$ (here the x -profile χ_0 is ignored). This yields the spin precession $\langle\psi|\sigma_y|\psi\rangle \propto \cos(\phi(y) + \phi_0)$ with the phase $\phi(y) = (k_+ - k_-)y$ as illustrated in Fig. 1(c). Physical implication of the phase is made explicit by rewriting $\phi(y)$ as

$$\phi(y) = \omega_L y / |\mathbf{v}_g|, \quad (1)$$

where $\omega_L = |g\mu_B B|/\hbar$ is the Larmor frequency and $|\mathbf{v}_g| = (1/\hbar)|g\mu_B B/\Delta k|$ with $\Delta k = k_- - k_+$. Equa-

tion (1) indicates that the phase of precession is experimentally controlled by B through ω_L as well as by V_{SG} through $|\mathbf{v}_g|$.

Similar coherent scattering takes place at the right-hand corner ($y = L$). The total transmission probability is given by the projection of $|\psi(L)\rangle$ onto the “probed state”, $|f\rangle = R_x(+\theta_1)|\uparrow\rangle$, in the up-spin branch of outgoing edge states:

$$T_{\uparrow\uparrow} = |\langle f|\psi(L)\rangle|^2 = \left| \langle \uparrow | S_R \begin{pmatrix} e^{ik_+y} & 0 \\ 0 & e^{ik_-y} \end{pmatrix} S_L | \uparrow \rangle \right|^2 = C_0 + C_1 \cos(\phi(L) + \phi_0). \quad (2)$$

The offset C_0 , the amplitude C_1 , and the phase offset ϕ_0 are constants determined by the scattering matrices S_L and S_R at the side-gate corners[26]. The phase of precession at $y = L$ is hence detected from the oscillation in $T_{\uparrow\uparrow}$.

By noting $\Delta k = -\Delta x/\ell_B^2$ with $\Delta x = x_- - x_+$, we can also express ϕ as the Aharonov-Bohm phase

$$\phi(L) = 2\pi BL\Delta x/(h/e), \quad (3)$$

determined by the number of magnetic flux quanta threading through the narrow stripe enclosed by the co-propagating edge states. This leads us to the equivalent interpretation in terms of the Mach-Zehnder type interferometer (see Fig. 1(d)[13]), where $T_{\uparrow\uparrow}$ oscillates as a result of the interference of two paths between “beam splitters” represented by the scattering matrices S_L and S_R . This system thus serves as a spin filtering device based on the two-path interference[28].

Oscillations in $T_{\uparrow\uparrow}(B)$ for different values of V_{SG} are analyzed with fast Fourier transform in a range of $B = 2.85\text{--}3.05\text{ T}$ [24], and the derived frequencies, ΔB^{-1} , are plotted against V_{SG} in the inset of Fig. 4(a). This confirms that ΔB^{-1} for $L = 10\text{ }\mu\text{m}$ is nearly twice as large as that for $L = 5\text{ }\mu\text{m}$. The values of ΔB^{-1} are translated into those of Δx through eq. (3) as shown in Fig. 4(a), which suggests that the spin-split inter-edge state distance is $\Delta x \sim 5\text{ nm}$ ($\ll \ell_B$).

These values of Δx are consistent with a theoretical expression $\Delta x \approx \sqrt{8|g\mu_B B|/\varepsilon\varepsilon_0/(\pi e^2 dn/dx|_{\nu=1})}$ with $\varepsilon = 13$ [29]. Here the electron density profile near the edge $n(x)$ is derived from an electrostatic model[30] and is plotted in Fig. 4(b) for different values of V_{SG} . Theoretical values of Δx are indicated with different lines in Fig. 4(a) for $g = -1.4, -2.9$, and -6.0 . Reasonable agreement with the experiment is obtained with $g = -2.9 \pm 0.1$, which is consistent with the exchange-enhanced g -factor at $\nu = 1$, estimated to be $g = -2 - 7$ in earlier experiments[31, 32]. (Note that the enhanced g -factor includes the effect of SOI[11].)

Closer look at the experimental data in Figs. 3(a) and 4(a) indicates that ΔB tends to decrease with increasing B and decreasing V_{SG} ($< -0.7\text{ V}$). These trends are also explained with a theoretically expected variation of Δx

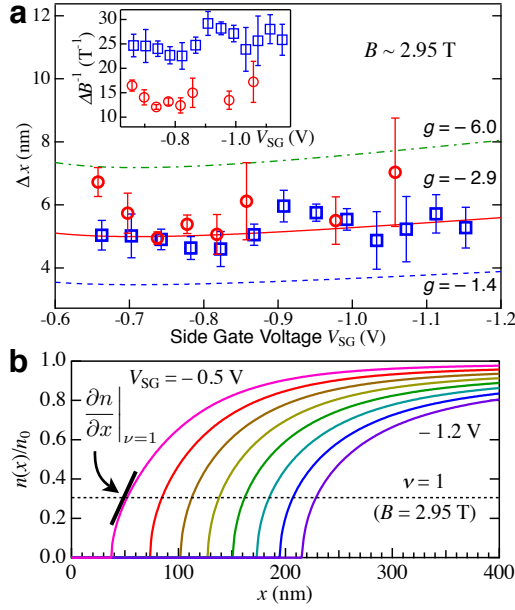


Figure 4. (Color online) (a) Inter-edge state separation Δx against V_{SG} for $L = 5 \mu\text{m}$ (red circles) and $L = 10 \mu\text{m}$ (blue squares), derived from ΔB^{-1} values in the inset. Dashed, solid, and dash-dotted lines represent theoretical values derived for $g = -1.4$, -2.9 , and -6.0 . The inset shows experimental values of ΔB^{-1} obtained from the oscillation in a range of $B = 2.85$ - 3.05 T. (b) Theoretically expected electron density distribution $n(x)$ for $V_{SG} = -0.5, -0.6, \dots, -1.2$ V[30]. Edge states are located at positions where $n(x)$ corresponds to $\nu = 1$, as indicated by the horizontal dashed line for $B \sim 2.95$ T.

(or ν_g): For instance, the profile of $n(x)$ in Fig. 4(b) shows that the confining potential becomes less steep and Δx increases as the edge states are pushed further away from the SG boundary with decreasing V_{SG} [30]. It is this dependence that gives rise to the oscillation against V_{SG} shown in the lower panel of Fig. 2(b).

Displayed in Fig 3(b) is a 2D plot of the theoretically predicted oscillatory pattern of $T_{\uparrow\uparrow}$ in a B - V_{SG} plane, which is derived from eq. (2) with $g = -2.9$, $C_0 = 0.92$, $C_1 = 0.08$, and $\phi_0 = 0$ [26]. Equipphase lines substantially reproduce the overall feature of experimental oscillations in Fig. 3(a). (The equipphase lines take broad maxima at $V_{SG} \approx -0.7$ V giving opposite slope on the side of $V_{SG} > -0.7$ V. This is consistent with the experiment and arises from the fact that the confining potential in Fig. 4(b) gets steeper as V_{SG} decreases for $V_{SG} > -0.7$ V[30].)

The experimental pattern in Fig. 3(a) suffers from irregular distortion. This is probably because long-range random potential affects the landscape of edge confining potential, giving rise to local fluctuations of Δx or v_g [24]. The area enclosed by the co-propagating trajectories of edge states, $L\Delta x$, or the phase $\phi(L)$ of spin precession, hence fluctuates as B or V_{SG} varies. Such long-range potential fluctuation, however, does not cause inter-edge

state scattering.

We note in Fig. 3(a) that $T_{\uparrow\uparrow}$ approaches unity and the amplitude of oscillation significantly diminishes as B increases beyond ~ 3.4 T. This implies that the scattering probability at the SG corners decreases at higher B . This is readily interpreted by noting that the potential at the side-gate corners becomes smoother due to screening by a wider compressible region of $0 < \nu < 1$ as B increases. The edge-state electrons in this regime adiabatically change their direction of motion in a smoothly curved potential without undergoing inter-edge state scattering[26]. The decrease of wave function overlap with increasing Zeeman splitting or decreasing ℓ_B may also suppress the scattering, but this effect was confirmed to be insignificant in our separate experiments with tilted magnetic fields.

The amplitude of oscillation corresponds to $C_1 \sim 0.04$ at $B \sim 3$ T in the experiment, which is smaller than but on the same order of the predicted value in the nonadiabatic limit[26]. This value is similar between the regions of $L = 5 \mu\text{m}$ and $10 \mu\text{m}$ (Fig. 2(b)) and confirmed to be independent of temperature up to ~ 160 mK. These findings suggest that the visibility of the oscillation is restricted by S_L and S_R in eq. (2) and the spin coherence length well exceeds $10 \mu\text{m}$ at 100 mK, which is noticeably larger than that of the orbital motion[13]. All-electrical coherent control of flying spins demonstrated in this work suggests that the edge states is a promising candidate for implementing flying spin qubits.

In conclusion, electrical control of spin precession in edge states has been demonstrated by converting gate-bias-induced static electric fields into spatially varying effective magnetic fields through the SOI. The phase of spin precession is controlled by B (through the Larmor frequency) or by V_{SG} (through the group velocity of electrons). We suggest an equivalent interpretation in terms of a Mach-Zehnder-type spin interferometer, in which the magnetic flux threading the area bounded by co-propagating spin-split edge states is controlled either by B or by $L\Delta x$. A ferromagnet-free spin-FET device has thus been experimentally demonstrated.

* nakajima@meso.t.u-tokyo.ac.jp; Present address: Department of Applied Physics, University of Tokyo, Hongo, Bunkyo-ku, Tokyo 113-8656, Japan

- [1] K. C. Nowack *et al.*, Science **318**, 1430 (2007).
- [2] S. Nadj-Perge *et al.*, Nature **468**, 1084 (2010).
- [3] S. Datta and B. Das, Appl. Phys. Lett. **56**, 665 (1990).
- [4] H. C. Koo *et al.*, Science **325**, 1515 (2009).
- [5] A. Bertoni *et al.*, Phys. Rev. Lett. **84**, 5912 (2000).
- [6] R. Ionićiu *et al.*, Int. J. Mod. Phys. B **15**, 125 (2001).
- [7] T. Stace *et al.*, Phys. Rev. Lett. **93**, 126804 (2004).
- [8] V. Giovannetti *et al.*, Phys. Rev. B **77**, 155320 (2008).
- [9] C. W. J. Beenakker *et al.*, Phys. Rev. Lett. **91**, 147901 (2003).

- [10] P. Samuelsson *et al.*, Phys. Rev. Lett. **92**, 026805 (2004).
- [11] G. Müller *et al.*, Phys. Rev. B **45**, 3932 (1992).
- [12] S. Komiyama *et al.*, Phys. Rev. B **45**, 11085 (1992).
- [13] Y. Ji *et al.*, Nature **422**, 415 (2003).
- [14] M. Büttiker, Phys. Rev. Lett. **57**, 1761 (1986).
- [15] S. Komiyama *et al.*, Phys. Rev. B **40**, 12566 (1989).
- [16] B. J. van Wees *et al.*, Phys. Rev. Lett. **62**, 1181 (1989).
- [17] J. Wang *et al.*, Phys. Rev. B **69**, 085304 (2004).
- [18] A. Reynoso *et al.*, Phys. Rev. B **70**, 235344 (2004).
- [19] Y. Bao, Phys. Rev. B **72**, 245323 (2005).
- [20] M. Pala *et al.*, Phys. Rev. B **71**, 115306 (2005).
- [21] V. L. Grigoryan *et al.*, Phys. Rev. B **80**, 165320 (2009).
- [22] A. V. Khaetskii, Phys. Rev. B **45**, 13777 (1992).
- [23] D. G. Polyakov, Phys. Rev. B **53**, 15777 (1996).
- [24] See Supplemental Material for the detailed description of the device structures and the possible effects of impurities.
- [25] J. Miller *et al.*, Phys. Rev. Lett. **90**, 076807 (2003).
- [26] In the limit of sharp potential edge at the gate corner, a and b are determined so that $|i\rangle = a|+\rangle + b|-\rangle$. In this case, $C_1 \sim 0.08$ is derived for $B = 3$ T. In the opposite limit of smooth corner, $|i\rangle$ would adiabatically changes to $|+\rangle$; i.e., $C_1 = 0$ or no inter-edge state scattering takes place ($S_L = S_R = I$). The values of a and b are also influenced by random potential fluctuations in real devices.
- [27] D. Yoshioka, *The Quantum Hall Effect*, Springer Series in Solid-State Sciences, Vol. 133 (Springer, 2002).
- [28] A. Lopez *et al.*, J. Phys.-Condes. Matter **22**, 115303 (2010).
- [29] D. B. Chklovskii *et al.*, Phys. Rev. B **46**, 4026 (1992).
- [30] I. A. Larkin and J. H. Davies, Phys. Rev. B **52**, R5535 (1995).
- [31] R. J. Nicholas *et al.*, Phys. Rev. B **37**, 1294 (1988).
- [32] A. Usher *et al.*, Phys. Rev. B **41**, 1129 (1990).